applied sciences

MDPI

Article

Proximate Time-Optimal Servomechanism Based on Transition Process for Electro-Optical Set-Point Tracking Servo System

Qianwen Duan [1,2,3], Qiunong He [1,2,3], Yao Mao [1,2,3,*], Xi Zhou [1,2,3] and Qintao Hu [1,2,3]

1 Key Laboratory of Optical Engineering, Chinese Academy of Sciences, Chengdu 610209, China; dqw951361350@163.com (Q.D.); heqiunong_ioe@163.com (Q.H.); zhouxiee@mail.ustc.edu.cn (X.Z.); hqt0099@mail.ustc.edu.cn (Q.H.)
2 Institute of Optics and Electronics, Chinese Academy of Sciences, Chengdu 610209, China
3 University of Chinese Academy of Sciences, Beijing 100049, China
* Correspondence: maoyao@ioe.ac.cn; Tel.: +86-135-4787-8788

Received: 28 September 2019; Accepted: 25 November 2019; Published: 29 November 2019

check for updates

Abstract: Set-point tracking servo systems encounter the problem of the trade-off between the swiftness and smoothness in tracking task. To deal with this problem, the proximate time-optimal servomechanism based on transition process (PTSTP) is proposed in this paper. The PTSTP control scheme incorporates a transition process (TP) into the framework of proximate time-optimal servomechanism (PTOS) to eliminate the conservatism of the original PTOS without the controller changing. The target position signal amplitude and the ultimate ability of actuator are utilized to design the time-optimal TP to make the jumping target position signal turns to a smooth signal, which can significantly reduce system overshoot. Therefore, the system swiftness and smoothness performance are guaranteed by PTSTP. Then, the stability of the proposed method is analyzed theoretically. Finally, the experimental results show that the controlled system is able to track the target position signal with different amplitude fast and smoothly in an electro-optical set-point tracking servo system.

Keywords: set-point tracking; transition process; proximate time-optimal servomechanism

1. Introduction

Set-point tracking systems, such as hard disk drive reading systems [1], surface mount device placement systems [2], electro-optical tracking systems [3,4], as well as mechanical arm control systems, play an significant role in the field of modern industrial process and are widely applied in energy exploration [5], celestial target observation, space beam communication [6], and other fields [7–9]. These processes require certain fastness and smoothness in target pointing with different amplitudes. In consideration of fastness, the most natural choice is time-optimal control (TOC) under the framework of stability [10,11], which is bang-bang control, deriving from the minimum principle. The TOC control scheme uses the maximum control capability to achieve the fastest acceleration and deceleration process. However, the uncertainty of the controlled object and the measurement noise will cause the system to generate chattering between the maximum and minimum values [12]. Moreover, the system may diverge because of the low sampling frequency of sensors when using the maximum control capability. Therefore, TOC is not advisable in practical systems.

To overcome the shortcomings of TOC and improve the smoothness of the control system, a proximate time-optimal servomechanism (PTOS) is proposed [12,13]. PTOS indicates that when the system tracking error is large, the control law adopts bang-bang control. When the system tracking error becomes small, the control law switches to linear control instead of bang-bang control in TOC.

This operation can reduce the system chattering to a certain extent, but the system performance of swiftness will be deteriorated in exchange for partial smoothness improvement. The set-point tracking control performance is quite different as the amplitude of the target position signal changed. Therefore, the input signal is usually divided into a wide-range signal (WRS) and a small-range signal (SRS). The standard of division is determined by the amplitude of the target position signal and the linear controller parameters in PTOS. It is related to drive capability, natural frequency, and damping ratio in an actual system. The input signal belongs to the SRSs when only the linear part of PTOS applied as the control scheme. If the complete PTOS control scheme is directly used, the input signal is WRS. In this paper, WRSs refer to the input signal with an amplitude greater than 10° in an electro-optical set-optical tracking system. Correspondingly, SRSs are the input signal with an amplitude less than or equal to 10°.

In fact, the research of PTOS is still a topic of interest in academic publications, and its advancement in tracking signals at WSRs has been confirmed [14–18]. The linear control employed by the PTOS during the tracking of signals in SRSs requires a compromise between swiftness and smoothness. Therefore, when using PTOS to track a SRS, there is still much room for improvement in system performance. The authors of [15] proposed a dynamically damped PTOS to nearly eliminate the conservatism of the original PTOS, which is combined with composite nonlinear feedback (CNF). When the input signal is a SRS, the linear feedback part of CNF is used to achieve the swiftness of response, and the nonlinear feedback part makes the system damping ratio in a changing state to get a better dynamic performance. However, the range of the input signal is limited by the parameters of the controller, and the controller parameter values need to be adjusted for different input signals to achieve the expected performance. When applying the control scheme into an actual system, the cumbersome parameter tuning cannot be ignored. To improve the set-point tracking performance of the PTOS control scheme in a SRS, Zhou et al. [18] proposed proximate time-optimal sliding-mode control scheme, which uses time-varying sliding surface and a third-order velocity profile to reduce the settling time; however, the paper does not analyze the system stability. In [19], the PTOS is applied to the hard disk drive system, and the experimental results at 180 degrees, 360 degrees, and 720 degrees set-point tracking indicate the swiftness, smoothness, and accuracy of the control scheme. However, the response performance to SRSs is not analyzed by this method, and the controller switching time is extremely difficult to determine. It is difficult to apply it to systems that have a strong demand for SRSs tracking. A PTOS control scheme based on damping ratio scheduling is proposed in [20], which uses adaptive velocity gain to achieve variable damping ratio of system, but the description of system stability is also not covered.

On the other hand, facing the control input saturation in SRS tracking when the process encounters the model uncertainty, the authors of [21] proposed a new anti-windup compensator for an uncertain linear system, which is the three degrees of freedom (3-DOF) structure composed of the controller, prefilter, and anti-windup compensator. Specifically, it is necessary to consider the Horowitz-Sidi bounds of the 3-DOF at the same time in Nichols chart to obtain the anti-saturation compensator. From the perspective of data-driven methods, the authors of [22] proposed a model-free neural network (NN)-based control scheme in an Adaptive Actor-Critic (AAC) learning framework. The initial controller for AAC designs is obtained from input-state-output data collected of the process in open-loop setting. Then the resulting suboptimal state-feedback controller is next improved under the AAC learning framework by online adaptation of a critic NN and a controller NN. In [23], the traditional two step anti-windup control methodology is applied to multiagent systems and the input constrained consensus tracking problem is solved based on distributed anti-windup compensator design. In this paper, the transition process (TP) is employed by recalculating the reference input signal. The controller can follow the new reference input without entering the saturation region, which ensures that the controller input is always equal to actuator output, thereby eliminating the windup phenomenon. Specifically, the TP is derived using the optimal control theory, and the performance index is the time optimum to maintain its swiftness. The derivation results show that the TP can be designed by the target position signal of any amplitude and the limit performance of actuator, which imply the design method is universal.

In the view of above discussions, the control scheme novelty and contributions of this paper is as follows.

(1) A proximate time-optimal servomechanism based on transition process (PTSTP) control scheme is proposed to reduce transition time and avoid big chatter simultaneously in set-point tracking processes, which incorporates a TP into the framework of PTOS. Furthermore, the stability region of PTSTP control scheme is proved. Finally, the proposed methodology is verified in an electro-optical set-point tracking system with inertial sensor-based closed loop.

(2) Compared with other improved PTOS control schemes, the PTSTP completely separates the design of the closed loop controller and the TP, which reduces much of the complex controller design work. Moreover, PTSTP has no limitations on the amplitude of the target position signal, which fully reflects the effectiveness of the control scheme for set-point tracking in the whole range.

(3) On the other hand, the design of TP is also an anti-windup method in essence. Compared with the former methods, it focuses on the processing of input signals rather than a back-calculation structure. It provides the engineers another choice to anti-windup, which can be directly added to the closed-loop outside according to the positioning amplitude and the limit performance of actuator.

The rest of this paper is organized as follows. In Section 2, we elaborate on the theoretical derivation of the standard PTOS and the analysis of the control algorithm. The PTSTP control scheme is shown in Section 3. In Section 4, we model the electro-optical set-point tracking control system, then verify the control scheme of PTSTP and analyze the experimental data in detail. Finally, a summary and outlook are given in Section 5.

2. PTOS Control Scheme

In this section, we simply introduce the control scheme of PTOS. As many typical servo systems can be modeled by double integral operators, the specific expression is depicted as

$$\begin{cases} \dot{x} = Ax + Bu \\ y = Cx \end{cases} \tag{1}$$

with

$$x = \begin{pmatrix} y \\ v \end{pmatrix}, A = \begin{bmatrix} 0 & 1 \\ 0 & 0 \end{bmatrix}, B = \begin{bmatrix} 0 \\ a \end{bmatrix}, C = \begin{bmatrix} 1 & 0 \end{bmatrix},$$

where x is the system state and A, B, C are the system state matrices. State y is the system position output, and v is the system speed output. u is the control input, which is also the control law output, and a is the positive acceleration constant.

To take the effects of control input saturation into account, u should be expressed as shown

$$u = \text{sign}(u_c) \cdot \min\{u_{\max}, |u_c|\}, \tag{2}$$

where u_c is the original output of the control law.

For the double integral operators, the goal of PTOS control scheme is to make the system output y track the target position signal r as quickly, accurately, and smoothly as possible, and the control law u_p is

$$u_p = \text{sign}(u) \cdot \min\{u_{\max}, |u_{out}|\}. \tag{3}$$

u_{out} is given by

$$u_{out} = k_2 [f(e) - v] \tag{4}$$

$$f(e) = \begin{cases} \frac{k_1}{k_2} e, & |e| \le y_L \\ \operatorname{sign}(e) \left[\sqrt{2a\alpha u_{\max} |e|} - J \right], & |e| > y_L \end{cases}, \tag{5}$$

where $e = r - y$ is the system positioning tracking error, and k_1 and k_2 represent the position feedback gain and speed feedback gain, respectively. The coefficient α can be regarded as the acceleration discount factor, and its value range is $\alpha \in [0.9, 0.99]$ for system robustness [13]. The variable y_L is the width of the linear control region and J is the offset to be determined. As $f(e)$ is composed of two parts—continuity and smoothness—$f'(e)$ and $f(e)$ should satisfy (6) at y_L.

$$\begin{cases} \frac{k_1}{k_2} y_L = \sqrt{2a\alpha u_{\max} |y_L|} - J \\ \frac{k_1}{k_2} = \sqrt{\frac{a\alpha u_{\max}}{2y_L}} \end{cases} \tag{6}$$

The linear feedback coefficients k_1, k_2 are determined by the pole configuration. The natural frequency and damping ratio of the closed-loop system are selected as ω_n and ζ according to the open-loop system requirement for phase margin and the gain margin in the practice engineering, which are supposed to have at least 45° and 6 dB. Then, k_1, k_2, J and y_L are calculated, respectively, as

$$k_1 = \frac{{\omega_n}^2}{a}, k_2 = \frac{2\zeta\omega_n}{a}, \tag{7}$$

$$J = \frac{a\alpha\zeta u_{\max}}{\omega_n}, \tag{8}$$

$$y_L = \frac{2\zeta J}{\omega_n}. \tag{9}$$

As the PTOS control scheme consists of three parts: saturation control, unsaturated control, and linear control, it enhances the system performance of swiftness and smoothness through the synergy of three parts. Saturation control means that when the system tracking error is large, the PTOS adopts the bang-bang control strategy. The maximum drive capability $u_{\max}$ of the actuator is used to accelerate, and the linear control means that when the system tracking error is gradually dropped below y_L, the controller switches to closed-loop control to make the system output asymptotic approach to the target position signal. To make the controllers switch smoother, the unsaturated control is used to connect the saturation control and linear control, which is reflected in the value of α in Equation (5). As can be seen from the above description, in the saturation control region, the system behaves as the optimal performance of the TOC. Meanwhile, the linear control region makes the control performance always compromised between the settling time and overshoot.

3. PTSTP Control Scheme

3.1. Limitations of PTOS Control Schemes in Tracking SRSs

The PTOS control scheme is widely used in set-point tracking scenarios for the WRSs [19,24] because of its rapidity, and it can be seen from Section 2 that when the application scenario is a SRS, the control law of PTOS is

$$\begin{aligned} u_{p\_small} &= k_2 [f(e) - v] \\ &= k_1 e - k_2 v \end{aligned}. \tag{10}$$

$$G_{open\_loop}(s) = \frac{a(k_2 s + k_1)}{s^2} = \frac{k(Ts+1)}{s^2} \tag{11}$$

When control law of Equation (10) is applied to the double integral object as in Equation (1), the system open-loop transfer function is shown in Equation (11), implying the system type number is II (type number is the number of integral links). At this point, the system will encounter two situations: First, designing parameters k_1 and k_2 is necessary for the system, which will make the trade-off between the overshoot and response settling time. Second, due to the windup phenomenon (The so-called windup refers to the phenomenon that the closed-loop performance of the system is deteriorated due to the unequal control input and actuator output) [25,26], the relative stability of the system may decrease. According to the classical linear control theory, the requirement of phase margin is usually higher than 45°. As show in Figure 1, the solid black line represents a simple Bode diagram of the Type II system, where ω_c is the system open-loop crossover frequency, γ is the system phase margin, and ω_a, ω_b are the frequency values corresponding to a phase margin of 45° in the phase-frequency curve.

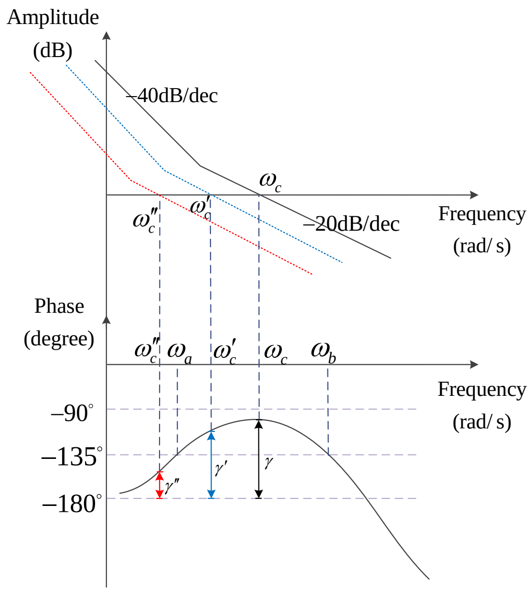

Figure 1. A simple Bode diagram of the Type II system.

When the system input signal is a SRS, the system error signal will encounter windup with a high probability. If so, the controller input is saturated, which equivalent to the system gain's (k Value in (11)) reduction. Correspondingly, the system amplitude–frequency curve will change from the solid black line to the blue dotted line or even the red dotted line in Figure 1. In the blue dotted line, the system phase margin is γ'. By comparing γ and γ', we can see that the relative stability of the system is declined, but γ' still meets the stability margin requirement in actual engineering. If the system gain k decreases so that the crossover frequency becomes ω_c'', the phase margin γ'' will be lower than 45°. At this time, the dynamic performance of the system is poor and the adaptability to the control system parameters is weak. As can be seen from the above analyses of the frequency response, the windup phenomenon can be regarded as an uncertain gain in the open loop transfer function. Due to the consistency of the frequency and time domain, the output signal may encounter oscillations or divergence after actuator saturated when the reference is a step/constant signal.

3.2. TP-Transition Process

To improve the performance of the PTOS control scheme for set-point tracking of SRSs, that is, to increase the swiftness and smoothness while avoiding windup, the TP is introduced in detail, which causes the jumping input signal r to become a slowly varying rising signal r_{tp}. After the system input becomes the TP signal r_{tp}, the control law will always calculate the control input depending on small errors, which completely avoids the windup to reduce the overshoot. By performing TP operation on the SRS, r_{tp} is obtained. And the control law of the PTOS for the SRSs in Equation (10) is integrated into Figure 2, where the new system can be rewritten as

$$\begin{cases} \dot{x} = (A - BK)x + Bk_1 r_{tp} \\ y = Cx \end{cases} \tag{12}$$

with

$$x = \begin{pmatrix} y \\ v \end{pmatrix}, A = \begin{bmatrix} 0 & 1 \\ 0 & 0 \end{bmatrix}, B = \begin{bmatrix} 0 \\ a \end{bmatrix},$$
$$C = \begin{bmatrix} 1 & 0 \end{bmatrix}, K = \begin{bmatrix} k_1 & k_2 \end{bmatrix}.$$

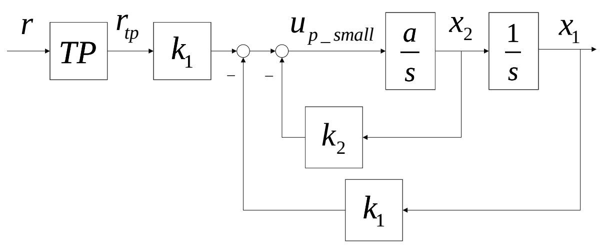

Figure 2. The control block of tracking SRSs after TP added into the PTOS.

The TP signal in Equation (12) is designed to track the SRSs fast and smoothly. The block diagram is shown in Figure 3, where r_{tp} tracks r, $\dot{r}_{tp} = r'_{tp}$.

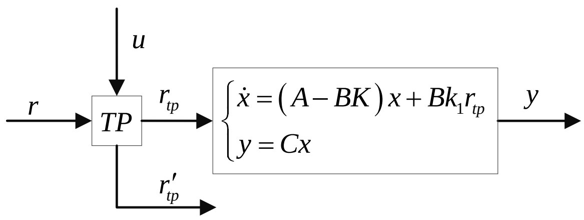

Figure 3. The control block for solving TP.

The method of solving TP is the minimum principle in the optimal control, wherein the time-optimal tracking is the performance index and the state r_{tp} is obtained by solving u. The TP portion in Figure 3 is

$$\begin{cases} \dot{z} = f(z, t) = A'z + B'u \\ y = C'z \end{cases} \tag{13}$$

with

$$z = \begin{pmatrix} z_1 \\ z_2 \end{pmatrix} = \begin{pmatrix} r_{tp} \\ r'_{tp} \end{pmatrix}, A' = \begin{bmatrix} 0 & 1 \\ 0 & 0 \end{bmatrix}, B' = \begin{bmatrix} 0 \\ 1 \end{bmatrix}, C' = \begin{bmatrix} 1 & 0 \end{bmatrix}.$$

The initial conditions and terminal conditions are, resepectively,

$$\begin{aligned} &z_1(0) = z_2(0) = 0, \\ &z_1\left(t_f\right) = r_A, z_2\left(t_f\right) = 0, \end{aligned} \tag{14}$$

where r_A is the absolute amplitude of input signal. And the control constraint is

$$|u| \le a_{\max}, 0 \le t \le t_f. \tag{15}$$

The objective is to solve the optimal control that minimizes the following performance index,

$$J = \varphi\left(z\left(t_f\right), t_f\right) + \int_{t_0}^{t_f} F\left(z\left(t\right), u\left(t\right), t\right) dt. \tag{16}$$

According the optimal control theory performance index design method in [27], we can choose $F = 1$ as a usually used, convenient and effective functional for time optimum design, and $\varphi = 0$ without considering the energy and fuel minimum. Then take the Hamilton function as

$$H = F + \lambda^{\mathrm{T}} f\left(z, t\right) = 1 + \lambda_1 z_2\left(t\right) + \lambda_2 u\left(t\right), \tag{17}$$

where λ is the co-state vector and expressed as

$$\lambda\left(t\right) = \left[\begin{array}{cc} \lambda_1\left(t\right) & \lambda_2\left(t\right) \end{array}\right]^T.$$

From the co-state equation

$$\begin{cases} \dot{\lambda}_1\left(t\right) = -\frac{\partial H}{\partial z_1} = 0 \\ \dot{\lambda}_2\left(t\right) = -\frac{\partial H}{\partial z_2} = -\lambda_1 \end{cases} \tag{18}$$

we can obtain

$$\begin{cases} \lambda_1\left(t\right) = c_1 \\ \lambda_2\left(t\right) = -c_1 t + c_2 \end{cases}, \tag{19}$$

where c_1 and c_2 is the integral constant. The optimal control $u\left(t\right)$ when taking the minimum value of H should be taken

$$u^*\left(t\right) = -a_{\max} \cdot \operatorname{sign}\left[\lambda_2\left(t\right)\right]. \tag{20}$$

It can be obtained from Equation (20), the function of $u\left(t\right)$ is a switching function, and the time of switching depends on the sign of $\lambda_2\left(t\right)$. When $0 \le t \le t_f$, $\lambda_2\left(t\right)$ should have both positive and negative value. Moreover, $u\left(t\right)$ should be $a_{\max}$ before the first switch. Therefore, the coefficient of $\lambda_2\left(t\right)$ should satisfy the condition $c_1 < 0, c_2 < 0$. Now, suppose $\lambda_2\left(t_1\right) = 0$, that is, $0 < t_1 < t_f$, then

$$u^*\left(t\right) = \begin{cases} a_{\max}, & 0 \le t \le t_1 \\ -a_{\max}, & t_1 \le t \le t_f \end{cases}. \tag{21}$$

From the equation of $\dot{z}_2\left(t\right) = u\left(t\right)$, combined with Equation (14), the state $z_1{}^*$ is

$$z_1{}^*\left(t\right) = \begin{cases} \frac{a_{\max}}{2} t^2, & 0 \leqslant t \leqslant t_1 \\ -\frac{a_{\max}}{2}\left(t - t_f\right)^2 + r_A, & t_1 < t \leqslant t_f \end{cases} \tag{22}$$

with

$$t_1 = \sqrt{\frac{r_A}{a_{\max}}}, t_f = \sqrt{\frac{4 r_A}{a_{\max}}}.$$

Now, we have obtained the r_{tp} signal by minimum principle as shown in Equation (23), and the signal diagram is shown in Figure 4, which completes the implementation of the jumping signal to the slowly changing signal. The performance index of the derivation process is time optimum, which is to minimize the response time of the system in Equation (12). Furthermore, r_{tp} always makes the system tracking error small, which greatly reduces the overshoot, avoids the windup phenomenon, and achieves fast and smooth tracking performance. Note that the design of r_{tp} is universal; that is, for a target position signal of any amplitude, the TP signal can be obtained on the premise that the ultimate acceleration ability of the control system actuator is known.

$$r_{tp}(t) = \begin{cases} \frac{a}{2}t^2, & 0 \leqslant t \leqslant t_1 \\ -\frac{a}{2}\left(t - t_f\right)^2 + r_A, & t_1 < t \leqslant t_f \\ r_A, & t_f < t \end{cases} \tag{23}$$

with

$$a = a_{\max}, t_1 = \sqrt{\frac{r_A}{a_{\max}}}, t_f = \sqrt{\frac{4r_A}{a_{\max}}},$$

where r_A is the absolute amplitude of input signal.

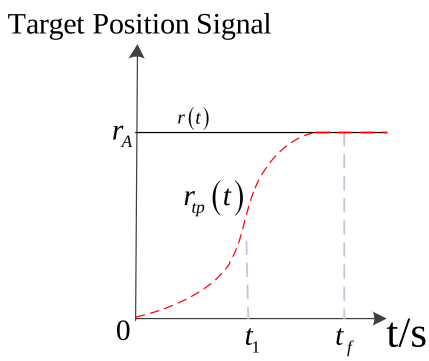

Figure 4. The comparison diagram of the step and the TP signal for positive value of r_A.

3.3. Summary of PTSTP Control Scheme

The PTSTP control block diagram is shown in Figure 5, and the control scheme is described as Equation (24), where u_t is the control law of PTSTP.

$$\begin{cases} \dot{y} = v \\ \dot{v} = au_t \end{cases} \tag{24}$$

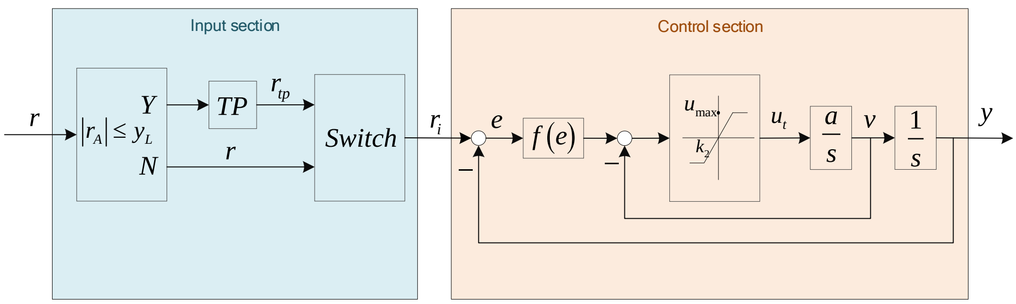

Figure 5. The control scheme of proximate time-optimal servomechanism based on transition process (PTSTP).

The block diagram consists of the input section and control section. The operation of the input section is to determine whether the input target position signal is a SRS or WRS according to the absolute value of step input. When it is a SRS, the Switch module in Figure 5 makes $r_i = r_{tp}$, whereas $r_i = r$ for the input signals belonging to WRS. The mathematical expression of Switch model is shown in the Equation (25), which means the WRS is not processed as a r_{tp}.

$$r_i(t) = \begin{cases} r_{tp}(t), & |r_A| \leq y_L \\ r(t), & |r_A| > y_L \end{cases} \tag{25}$$

Then the control law u_t is selected by r_i, which means that u_t is the control law of u_{p_small} for $r_i = r_{tp}$, whereas u_t is the control law of u_{p_wide} for $r_i = r$. The expression is shown in the Equation (26), where u_{p_small} and u_p are the control law of PTOS for SRSs and WRSs tracking, respectively.

$$u_t = \begin{cases} u_{p\_small}, & r_i = r_{tp} \\ u_{p\_wide} = u_p, & r_i = r \end{cases}, \tag{26}$$

where u_{p_small} and u_p are equivalent to Equations (10) and (3), respectively.

3.4. The Stability Region of PTSTP Control Scheme

According to the work in [28], the system stability analysis of PTSTP control scheme using Appendix A is as follows.

Theorem 1. *The PTSTP control scheme is globally asymptotically stable if the following conditions hold.*

(1) $k_2 > 0$.
(2) $k_1 > \frac{1}{a}$.
(3) $f(0) = 0$.
(4) $f(z)z > 0, \forall z \neq 0$.
(5) $f'(y) \triangleq df(y)/dy\, exist, \forall y$.
(6) $-a + \frac{1}{k_2} f'(-y) < -f'(-y) f(-y) < a - \frac{1}{k_2} f'(-y), \forall y$.

The $f(\cdot)$ is associated with Equation (5).

Proof. When the PTSTP control scheme is tracking SRSs, the time-invariant system in Figure 2 and Equation (12) can be described as

$$\dot{x} = \begin{bmatrix} 0 & 1 \\ -ak_1 & -ak_2 \end{bmatrix} x + \begin{bmatrix} 0 \\ ak_1 \end{bmatrix} r_{tp} \tag{27}$$

with

$$x = \begin{bmatrix} y \\ v \end{bmatrix}, \dot{x}(0) = 0.$$

Select the positive scalar function $V(x)$ as follows.

$$V(x) = {x_1}^2 + {x_2}^2 \tag{28}$$

As the input signal does not change the stability of the system and the derivative of $V(x)$ along with any trajectory is

$$\begin{aligned} \dot{V}(x) &= 2x_1\dot{x}_1 + 2x_2\dot{x}_2 \\ &= -2ak_2{x_2}^2 + 2x_1x_2(1 - ak_1). \end{aligned} \tag{29}$$

when $1 - ak_1 < 0$ and $k_2 > 0$, $\dot{V}(x)$ is negative in Equation (29). This shows that $V(x)$ decreases continuously along with any trajectory. At this condition, when $\|x\| \to \infty, V(x) \to \infty$. Therefore, using the approach of Lyapunov stability in Appendix A, in the case of $k_1 > 1/a$, $k_2 > 0$, the system equilibrium state is globally asymptotically stable.

Moreover, the PTSTP control scheme should meet conditions (3–6) in Theorem 1 when tracking WRSs. The proof of this is rather long and is found in [12].

Thus, Theorem 1 is proved. □

4. Application in Electro-Optical Tracking System

The electro-optical tracking device is mainly composed of the main control, servo system, sensors, data acquisition and forwarding unit. After receiving the target position signal sent by the control center unit, the servo system drives the motor to perform set-point tracking. As the system pointing error decreases, the target will gradually appear on the image sensor. The schematic diagram of the servo system is shown in Figure 6. It consists of the azimuth axis and the elevation axis, and is fixed on the ground. The servo system achieves the purpose of fast, smooth, and accurate set-point tracking by controlling the azimuth and elevation angles of the device. As the azimuth axis and the elevation axis have the same control mode, and the control method of the positive direction and the opposite direction of each axis is exactly the same, this paper takes the azimuth axis forward control as an example to analyze the control method of the electro-optical tracking system. Thereby, the range of the servo system target position signal is $(0^\circ, 180^\circ]$.

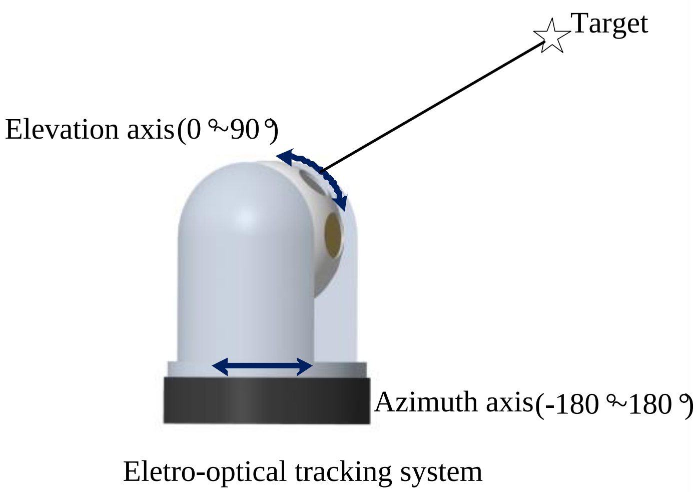

Figure 6. The schematic diagram of electro-optical tracking system.

To improve the rigidity of the inner loop [3], the microelectromechanical system's (MEMS) gyroscope is installed in the electro-optical servo system for speed measurement, which uses the speed signal to achieve a speed closed-loop. Therefore, the controlled object is an integral element connecting with a first-order inertia element, such as in Equation (30).

$$\begin{cases} \dot{x} = Ax + Bu_t \\ y = Cx \end{cases} \tag{30}$$

with

$$x = \begin{pmatrix} y \\ v \end{pmatrix}, A = \begin{bmatrix} 0 & 1 \\ 0 & -\frac{1}{T} \end{bmatrix}, B = \begin{bmatrix} 0 \\ \frac{b}{T} \end{bmatrix},$$
$$C = \begin{bmatrix} 1 & 0 \end{bmatrix}, |u| \leqslant u_{\max},$$

where b, T are the parameters of the controlled object.

Then, the control scheme PTSTP is applied to the electro-optical servo system, and its expression for input section is

$$r_i = \begin{cases} r_{tp}, & |r_A| \leqslant r_0 + y_L \\ r & |r_A| > r_0 + y_L \end{cases}. \tag{31}$$

To ensure the consistency of the system type number when applying the linear controller, the proportional differential controller of Equation (26) becomes the proportional integral controller of Equation (32). The control section is

$$\begin{aligned} & u_t = \begin{cases} u_{p\_small}, & r_i = r_{tp} \\ u_{p\_wide}, & r_i = r \end{cases}, \\ & u_{p\_small} = k_p e + k_i \int e\,\mathrm{d}t, \\ & u_{p\_wide} = \mathrm{sign}\,(u) \cdot \min\{u_{\max}, |u_{out}|\}, \\ & u_{out} = \begin{cases} k_p e + k_i \int e\,\mathrm{d}t, & |e| \le y_L \\ \mathrm{sign}\,(e) \cdot u_{\max}, & |e| > y_L \end{cases}, \\ & y_L = \frac{u_{\max}}{k_p}\,(u_{\max} = v_{\max}), \end{aligned} \tag{32}$$

where k_p, k_i represent the proportional coefficient and the integral coefficient, respectively, and are adjusted according to system stability and dynamic response [29]. As the motor speed is limited in the real system, it is tentatively set r_0 to the angle at which the system speed is increased from 0 to $v_{\max}$. Comparing the control law of single integral and double integral, it is found that Equation (31) has one small difference with Equation (25). When the amplitude of input signal is slightly bigger than y_L, the control law of u_{p_wide} will bring some chattering to the system, and the operation of *when* $|r_A| \leqslant r_0 + y_L, r_i = r_{tp}$ will increase the elastic space of r_0.

The experimental platform of the electro-optical servo system is shown in Figure 7, which consists of a MEMS gyroscope, an encoder signal processing board, and a permanent magnet DC torque motor. The DC torque motor parameters are shown in Table 1. The MEMS gyro is used to measure the angular speed, and the absolute rotary electro-optical encoder is applied to measure the angle value within the range of $[-180°, 180°]$. The MEMS gyroscope is applied to form an inertial closed loop, improving the characteristics of the controlled object and rejecting the nonlinearity, which also has been proved to be effective in stabilizing the system [30].

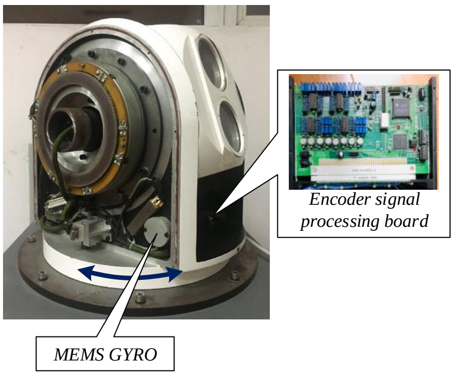

Figure 7. The experimental platform.

Table 1. Parameters of the motor.

Parameters	Units	Values
Rated voltage	V	60
Rated current	A	4.6
Rated torque	Nm	30
Torque constant	Nm/A	3.5
Stator inductance	mH	16.3
Stator resistance	Ω	11.5

The position controlled object after the velocity closed loop is shown in Figure 8, in which the solid blue line indicates the measured curve, and the red dotted line represents the fitted curve. The fitted curve shows that it is the first-order inertial link series integral link. Applying the PTSTP control scheme to the electro-optical servo system, the parameters of the controlled object in Equation (30) are

$$A = \begin{bmatrix} 0 & 1 \\ 0 & -25.126 \end{bmatrix}, B = \begin{bmatrix} 0 \\ 26.442 \end{bmatrix}$$
$$C = \begin{bmatrix} 1 & 0 \end{bmatrix}, |u| \leqslant 92^\circ/s.$$

The parameter in the control law Equation (32) is $k_p = 11.876, k_i = 6.15, y_L = 7.75^\circ, r_0 = 2.359^\circ$. The results of using the PTSTP control scheme for the WRSs in the electro-optical servo system is shown in Figure 9, in which the system position output is normalized. It can be seen that the overshoot can be made within $\pm 2\%$.

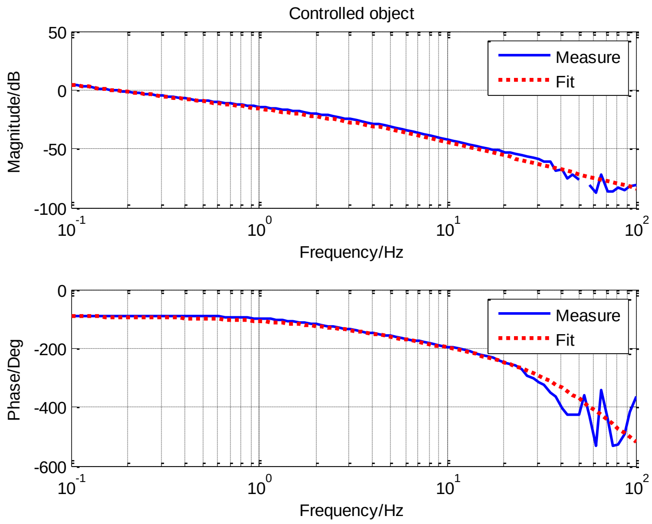

Figure 8. The Bode diagram of the controlled object.

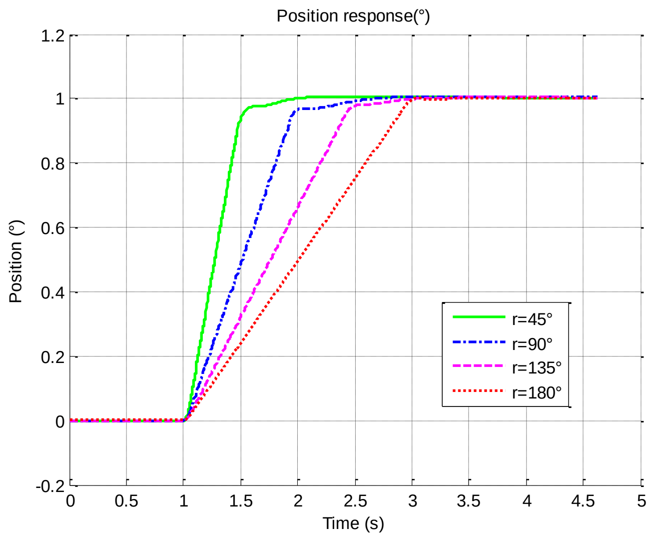

Figure 9. The wide-range signals (WRSs) set-point tracking normalization curve.

To observe the changes in the various states of the system when tracking the SRSs by using the PTOS and PTSTP control scheme, the tracking implementation of 10°, 5°, and 1° target position signals is shown in Figures 10–12, in which the r_{tp} is designed by Equation (23). The red dotted line represents the curve of each state when the system use PTSTP, and the blue solid line is using the PTOS. The subfigure (a) represents the position curve, (b) represents the speed curve, (c) represents the system tracking error, and (d) represents the input motor current curve, respectively. Finally, through data processing, the experimental results are summarized in Tables 2 and 3.

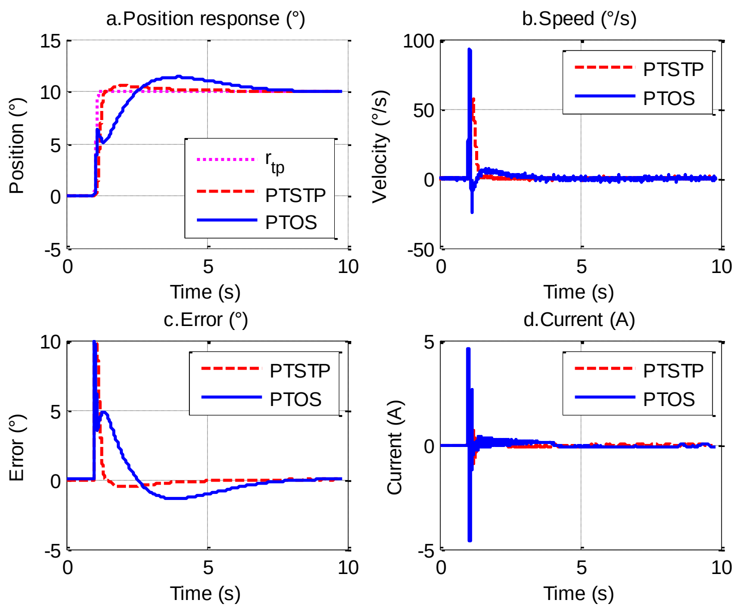

Figure 10. Comparison between PTSTP and PTOS tracking target position signal $r = 10°$.

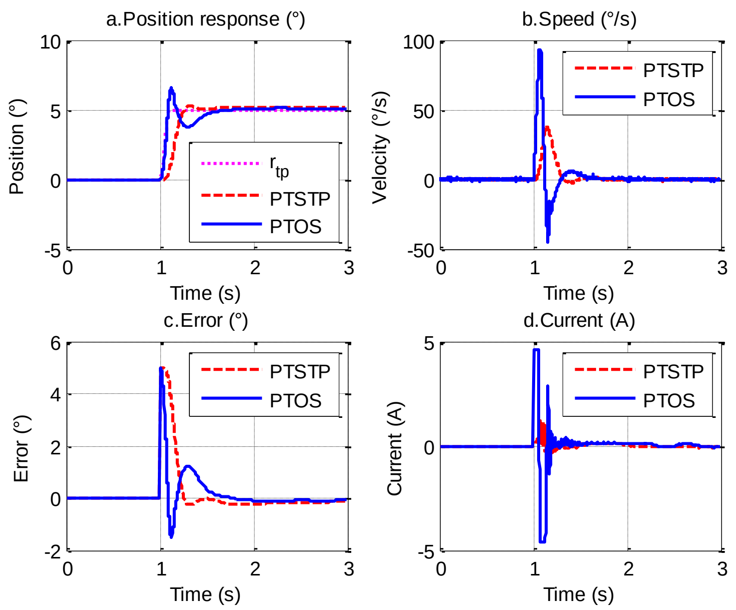

Figure 11. Comparison between PTSTP and PTOS tracking target position signal $r = 5°$.

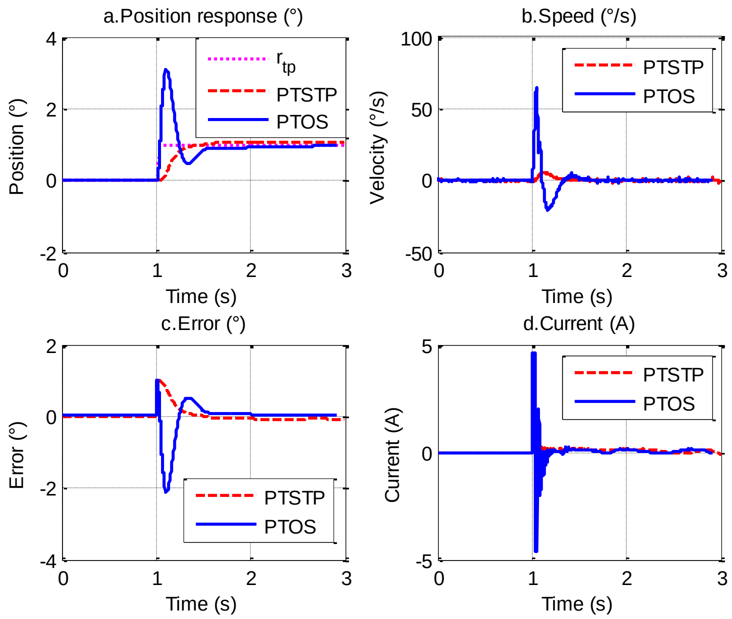

Figure 12. Comparison between PTSTP and PTOS tracking target position signal $r = 1°$.

Table 2. Settling time comparison

Signal Amplitude	Settling Time	
	PTSTP	PTOS
$r = 10°$	2.951	6.238
$r = 5°$	1.614	1.772
$r = 1°$	0.327	0.567

Table 3. Overshoot comparison

Signal Amplitude	Overshoot	
	PTSTP	PTOS
$r = 10°$	5.211%	13.874%
$r = 5°$	5.023%	17.832%
$r = 1°$	5.116%	210.501%

Note that the settling time in Table 2 is the minimum time required for the system position signal to reach and remain within the final value of ±2%. Considering the limited accuracy of the encoder, the settling time of 1° is calculated using the minimum time required for the system position signal to reach and remain within the final values of ±10%. First, from subfigure (d) of Figures 10–12, when the system use PTOS, the saturation of current output from the actuator indicates that the windup phenomenon occurs from the beginning of the control process, which is the reason for the large position overshoot. However, the position curve of PTSTP is smoother than PTOS, and the windup phenomenon is avoided because of the addition of TP. As can be seen from subfigure (a) in Figure 10, the oscillation phenomenon occurs at the early stage of the control process, which is the reason for the operation when $|r_A| \leqslant r_0 + y_L, r_i = r_{tp}$ in the control law Equation (32). It enhances the smoothness of the PTSTP control scheme applying to the single-integral series inertial objects in a certain extent. Second, as the amplitude of the input signal decreases, the overshoot of the PTOS algorithm becomes larger, even reaching an unacceptable level. However, the overshoot of PTSTP keeps near 5% in Table 2, and the settling time is obviously less than PTOS in Table 3. Although the advantage of settling time is not particularly obvious when tracking 5° signal, from the overall performance point of view, PTSTP is more advanced than the PTOS control scheme.

5. Conclusions

This paper proposes a PTSTP control scheme by embedding the TP in the framework of PTOS, and theoretically gives the region of system stability. After applying it to an electro-optical tracking system, the experimental data shows that the control scheme can track target position signals of different amplitude fast and smoothly. Therefore, it can be foreseen that the PTSTP control scheme will be widely used in set-point tracking servo systems in the future. Next work will concentrate on the friction modeling and compensation solution in set-point tracking.

Author Contributions: Conceptualization, Q.D. and Y.M.; Data curation, Q.D. and Q.H. (Qiunong He); Formal analysis, Q.D., Q.H. (Qintao Hu), and X.Z.; Funding acquisition, Y.M.; Investigation, Q.D., X.Z., and Y.M.; Methodology, Q.D. and Y.M.; Project administration, Q.D. and Y.M.; Software, Q.D. and Q.H. (Qiunong He); Supervision, Q.D. and Y.M.; Validation, Q.D.; Visualization, Q.D.; Writing—original draft, Q.D.; Writing—review & editing, Q.D., Q.H. (Qiunong He), X.Z., and Y.M.

Funding: This research received no external funding.

Acknowledgments: Comments and suggestions from Yao Mao, Qiunong He, Xi Zhou, Wei Ren, Zhijun Li, and Wei Yu during this study are very much appreciated.

Conflicts of Interest: The authors declare no conflicts of interest.

Abbreviations

The following abbreviations are used in this manuscript:

PTSTP	proximate time-optimal servomechanism based on transition process
PTOS	Proximate Time-optimal Servomechanism
CNF	Composite Nonlinear Feedback
TOC	Time Optimal Control
WRS	Wide Range Signal
SRS	Small Range Signal
TP	Transition Process

Appendix A. Lyapunov Global Asymptotic Stability Theorem

For a time-invariant system $\dot{x} = f(x), t \geq 0$, where $f(0) = 0$, if there is a scalar function $V(x)\,(V(0) = 0)$ with a continuous first derivative, and $V(x)$ satisfies the following conditions for all nonzero points x in the state space X, the origin equilibrium state of the system is globally asymptotically stable.

(1) $V(x)$ is positive.
(2) $\dot{V}(x)$ is negative.
(3) When $\|x\| \to \infty, V(x) \to \infty$.

References

1. Venkataramanan, V.; Chen, B.M.; Lee, T.H.; Guo, G. A new approach to the design of mode switching control in hard disk drive servo systems. *Control Eng. Pract.* **2002**, *10*, 925–939. [CrossRef]
2. Kim, J.H.; Choi, J.W.; Sul, S.K. High precision position control of linear permanent magnet synchronous motor for surface mount device placement system. In Proceedings of the Power Conversion Conference-Osaka 2002 (Cat. No. 02TH8579), Osaka, Japan, 2–5 April 2002; Volume 1, pp. 37–42.
3. Deng, C.; Mao, Y.; Ren, G. MEMS inertial sensors-based multi-loop control enhanced by disturbance observation and compensation for fast steering mirror system. *Sensors* **2016**, *16*, 1920. [CrossRef]
4. Ren, W.; Luo, Y.; He, Q.; Zhou, X.; Deng, C.; Mao, Y.; Ren, G. Stabilization control of electro-optical tracking system with fiber-optic gyroscope based on modified smith predictor control scheme. *IEEE Sens. J.* **2018**, *18*, 8172–8178. [CrossRef]

5. Rahman, S.; Ferdaus, R.A.; Mannan, M.A.; Mohammed, M.A. Design & implementation of a dual axis solar tracking system. *Am. Acad. Sch. Res. J.* **2013**, *5*, 47.
6. Yin, J.; Cao, Y.; Li, Y.H. Satellite-based entanglement distribution over 1200 kilometers. *Science* **2017**, *356*, 1140–1144. [CrossRef] [PubMed]
7. Perez-Arancibia, N.O.; Gibson, J.S.; Tsao, T.C. Observer-based intensity-feedback control for laser beam pointing and tracking. *IEEE Trans. Control Syst. Technol.* **2012**, *20*, 31–47. [CrossRef]
8. Liu, H.; Yu, H. Finite-Time Control of Continuous-Time Networked Dynamical Systems. *IEEE Trans. Syst. Man Cybern. Syst.* **2018**. [CrossRef]
9. Liu, H.; Wang, D. Stability and stabilisation of a class of networked dynamic systems. *Int. J. Syst. Sci.* **2018**, *49*, 964–973. [CrossRef]
10. Mayne, D.Q.; Schroeder, W. Robust time-optimal control of constrained linear systems. *Automatica* **1997**, *33*, 2103–2118. [CrossRef]
11. Sui, D.; Feng, L.; Ong, C. Interpolated robust time-optimal controllers for linear systems. *IET Control Theory Appl.* **2008**, *2*, 219–227. [CrossRef]
12. Workman, M.L.; Kosut, R.L.; Franklin, G.F. Adaptive proximate time-optimal servomechanisms: Continuous time case. In Proceedings of the 1987 American Control Conference, Minneapolis, MN, USA, 10–12 June 1987; pp. 589–594.
13. Workman, M.L.; Kosut, R.L.; Franklin, G.F. Adaptive proximate time-optimal servomechanisms: Discrete-time case. In Proceedings of the 26th IEEE Conference on Decision and Control, Los Angeles, CA, USA, 9–11 December 1987; Volume 26, pp. 1548–1553.
14. Chong, S.; Foo, J. Comparative Evaluation of Positioning Performance for a Direct Drive System: CM NCTF versus PTOS. In Proceedings of the 2018 15th International Conference on Control, Automation, Robotics and Vision (ICARCV), Singapore, 18–21 November 2018; pp. 1164–1169.
15. Flores, J.; Salton, A.; da Silva, J.G., Jr.; Neto, N.; Chen, Z. A discrete-time framework for proximate time-optimal performance of damped servomechanisms. *Mechatronics* **2016**, *36*, 27–35. [CrossRef]
16. Braker, R.A.; Pao, L.Y. Proximate time-optimal control of a second-order flexible structure. In Proceedings of the 2015 IEEE Conference on Control Applications (CCA), Sydney, Australia, 21–23 September 2015; pp. 840–845.
17. Salton, A.T.; Chen, Z.; Fu, M. Improved control design methods for proximate time-optimal servomechanisms. *IEEE/ASME Trans. Mechatron.* **2012**, *17*, 1049–1058. [CrossRef]
18. Zhou, J.; Zhou, R.; Wang, Y.; Guo, G. Improved proximate time-optimal sliding-mode control of hard disk drives. *IEEE Proc. Control Theory Appl.* **2001**, *148*, 516–522. [CrossRef]
19. Cheng, G.; Hu, J.G. An observer-based mode switching control scheme for improved position regulation in servomotors. *IEEE Trans. Control Syst. Technol.* **2014**, *22*, 1883–1891. [CrossRef]
20. Choi, Y.M.; Jeong, J.; Gweon, D.G. Modified damping scheduling proximate time optimal servomechanism for improvements in short strokes in hard disk drives. *IEEE Trans. Magn.* **2008**, *44*, 540–546. [CrossRef]
21. Jeyasenthil, R.; Choi, S.B. A new anti-windup compensator based on quantitative feedback theory for an uncertain linear system with input saturation. *Appl. Sci.* **2019**, *9*, 2958. [CrossRef]
22. Radac, M.B.; Precup, R.E. Data-Driven model-free tracking reinforcement learning control with VRFT-based adaptive actor-critic. *Appl. Sci.* **2019**, *9*, 1807. [CrossRef]
23. Fu, J.; Lv, Y.; Huang, T. Distributed anti-windup approach for consensus tracking of second-order multiagent systems with input saturation. *Syst. Control Lett.* **2019**, *130*, 1–6. [CrossRef]
24. Choi, Y.M.; Jeong, J.; Gweon, D.G. A novel damping scheduling scheme for proximate time optimal servomechanisms in hard disk drives. *IEEE Trans. Magn.* **2006**, *42*, 468–472. [CrossRef]
25. Tarbouriech, S.; Turner, M. Anti-windup design: An overview of some recent advances and open problems. *IET Control Theory Appl.* **2009**, *3*, 1–19. [CrossRef]
26. Tian, D.; Shen, H.; Dai, M. Improving the rapidity of nonlinear tracking differentiator via feedforward. *IEEE Trans. Ind. Electron.* **2014**, *61*, 3736–3743. [CrossRef]
27. Berkovitz, L.D. *Optimal Control Theory*; Springer Science & Business Media: New York, NY, USA, 2013; Volume 12.
28. Dorf, R.C.; Bishop, R.H. *Modern Control Systems*; Pearson: Upper Saddle River, NJ, USA, 2011.

29. Lennartson, B.; Kristiansson, B. Evaluation and tuning of robust PID controllers. *IET Control Theory Appl.* **2009**, *3*, 294–302. [CrossRef]
30. Tian, J.; Yang, W.; Peng, Z.; Tang, T. Inertial sensor-based multiloop control of fast steering mirror for line of sight stabilization. *Opt. Eng.* **2016**, *55*, 111602. [CrossRef]